ACS NANO
Cite This: ACS Nano 2019, 13, 10972−10979
www.acsnano.org

ARTICLE

Multimodal Sensing with a Three-Dimensional Piezoresistive Structure

Sang Min Won,[†,‡,&] Heling Wang,[§,⬢,∥,⊥,&] Bong Hoon Kim,[#,&] KunHyuck Lee,[∥,&] Hokyung Jang,[‡] Kyeongha Kwon,[⊥] Mengdi Han,[⊥] Kaitlyn E. Crawford,[⊗] Haibo Li,[§,⬢,∥,⊥] Yechan Lee,[‡] Xuebo Yuan,[§,⬢,∥,⊥] Sung Bong Kim,[‡,▽] Yong Suk Oh,[⊥] Woo Jin Jang,[‡] Jong Yoon Lee,[‡] Seungyong Han,[○] Jeonghyun Kim,[◆] Xueju Wang,[¶] Zhaoqian Xie,[%] Yihui Zhang,[◇] Yonggang Huang,[§,⬢,∥,⊥] and John A. Rogers[*,‡,■]

[†]Department of Electrical and Computer Engineering, [‡]Frederick Seitz Materials Research Laboratory, and [▽]Department of Materials Science and Engineering, University of Illinois at Urbana−Champaign, Urbana, Illinois 61801, United States

[§]Department of Mechanical Engineering, [⬢]Department of Civil and Environmental Engineering, [∥]Department of Materials Science and Engineering, and [⊥]Center for Bio-Integrated Electronics, Northwestern University, Evanston, Illinois 60208, United States

[#]Department of Organic Materials and Fiber Engineering, Smart Wearable Engineering, Information Communication Materials, and Convergence Technology, Soongsil University, 369 Sangdo-ro, Dongjak-gu, Seoul 06978, Republic of Korea

[⊗]Department of Materials Science and Engineering, University of Central Florida, Orlando, Florida 32816, United States

[○]Department of Mechanical Engineering, Ajou University, Suwon 16499, Republic of Korea

[◆]Department of Electronics Convergence Engineering, Kwangwoon University, Seoul 01897, Republic of Korea

[¶]Department of Mechanical and Aerospace Engineering, University of Missouri, Columbia, Missouri 65201, United States

[%]Department of Engineering Mechanics, Dalian University of Technology, Dalian 116024, China

[◇]Center for Flexible Electronics Technology and Center for Mechanics and Materials, AML, Department of Engineering Mechanics, Tsinghua University, Beijing 100084, China

[■]Center for Bio-Integrated Electronics, Departments of Materials Science and Engineering, Biomedical Engineering, Chemistry, Mechanical Engineering, Electrical Engineering and Computer Science, and Neurological Surgery, Simpson Querrey Institute for Nano/biotechnology, McCormick School of Engineering and Feinberg School of Medicine, Northwestern University, Evanston, Illinois 60208, United States

Supporting Information

ABSTRACT: **Sensors that reproduce the complex characteristics of cutaneous receptors in the skin have important potential in the context of artificial systems for controlled interactions with the physical environment. Multimodal responses with high sensitivity and wide dynamic range are essential for many such applications. This report introduces a simple, three-dimensional type of microelectromechanical sensor that incorporates monocrystalline silicon nanomembranes as piezoresistive elements in a configuration that enables separate, simultaneous measurements of multiple mechanical stimuli, such as normal force, shear force, and bending, along with temperature. The technology provides high sensitivity measurements with millisecond response times, as supported by quantitative simulations. The fabrication and assembly processes allow scalable production of interconnected arrays of such devices with capabilities in spatiotemporal mapping. Integration with wireless data recording and transmission electronics allows operation with standard consumer devices.**

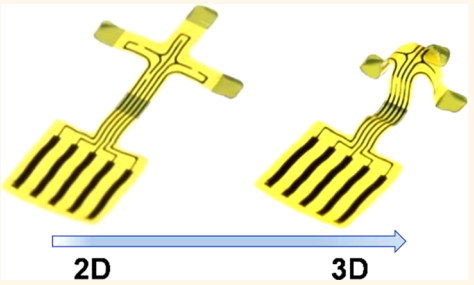

KEYWORDS: *tactile sensor, three-dimensional, electronic skin, silicon nanomembrane, electromechanical sensor*

Mechanoreceptors, nociceptors, and thermoreceptors are essential parts of the somatosensory system and are found throughout the body including at all areas across the surface of the skin. Such cutaneous sensory receptors play critical roles in detecting stimuli (e.g., mechanical and

Received: March 14, 2019
Accepted: May 9, 2019
Published: May 24, 2019

DOI: 10.1021/acsnano.9b02030
ACS Nano 2019, 13, 10972−10979

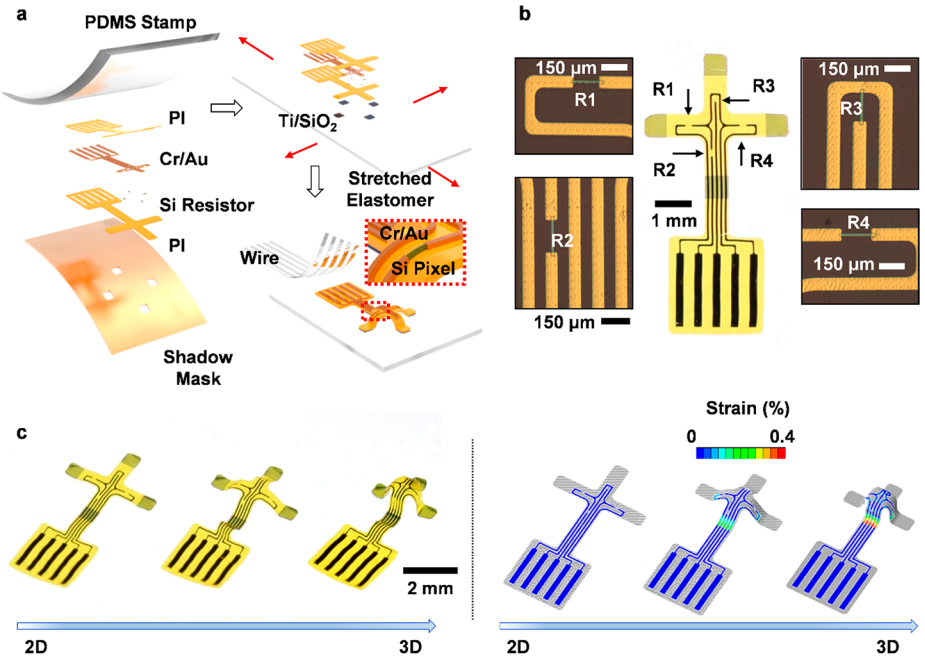

Figure 1. Materials and construction of a 3D piezoresistive sensor on an elastomer substrate. (a) Schematic illustration for the fabrication of the sensor after retrieval of a corresponding 2D precursor onto a PDMS stamp and deposition of Ti/SiO_2 onto defined sites on the backside (left). Transfer printing processes deliver this structure onto a prestrained silicone substrate (top right). Release of strain transforms the piezoresistive sensor in 3D table-like configuration (bottom right) via a buckling process. (b) Optical microscope images of 2D precursor that have two piezoresistors (R2 and R3) in the vertical direction and the other two (R1 and R4) in the horizontal direction. (c) Optical image (left frame) and computed distributions of strain (right frame) during the mechanical buckling processes.

thermal) from the surrounding physical environment. As such, man-made devices with similar capabilities and soft mechanical properties have widespread potential applications in health monitoring,[1−4] biomedical prosthetics,[5,6] electronic skin,[7−10] and human−machine interfaces.[11−14] Examples of tactile platforms include those capable of sensing pressure,[2−5,11] shear forces,[6,7,15] torsion deformations,[15−17] and temperature,[8,18] with high sensitivity and wide dynamic range. Many approaches exist for measuring the first and last parameters; the second and third are more challenging, although essential in reproducing shapes, textures, frictional forces, and other parameters needed for meaningful tactile sensing.

Research in this area combines exploratory efforts in materials science and device design, where physical transduction typically occurs via capacitive,[7−9,15] piezoelectric,[19−21] piezoresistive,[3,13,16−18] and/or triboelectric effects.[22−24] Materials ranging from ultrathin metallic wires,[17] silicon nanomembranes (Si-NMs),[3,18,25] carbon nanotubes[21,26] and liquid metals[2,27−29] to nanoparticles[30−32] and nanowires,[16,17,24] each on flexible and/or stretchable substrates, offer the necessary sensing performance in mechanically compliant architectures that are compatible with large-area fabrication. Most of these sensors, however, support measurements of only a single parameter, such as normal force (pressure)[1−5] or temperature;[3,8,18,33] several provide both,[8,18,33] but only a few have capabilities in recording shear and/or torsion deformations.[6,7,15−17] Recent research efforts attempt to address these limitations. For example, sensors based on interlocking arrays of Pt-coated nanofibers offer sensitivity to pressure, shear, and torsion,[16] but with responses that can be difficult to decouple for separate measurement of these quantities. Devices that incorporate microstructured pyramidal features of relief on elastomers represent additional examples of platforms with multifunctional tactile sensory capabilities.[7,15] Here, the devices can measure and discriminate between normal and shear forces but with linear responses that cover a relatively small dynamic range.

This report introduces a three-dimensional (3D) tactile sensor design that uses piezoelectric monocrystalline Si-NM elements integrated together in a soft platform that is capable of decoupled measurement of multiple external stimuli. The 3D structure takes the form of a table-like shape (planar top surface with four supporting legs) that results from mechanically guided geometry transformation of a two-dimensional (2D) planar precursor that incorporates four Si-NM elements at strategic locations across a patterned thin polymer film.[34−38] The resulting system provides high sensitivity via the large gauge factor of monocrystalline silicon in a 3D architecture that enables simultaneous recording of pressure, shear force, and bending strain, along with temperature. A key feature is the ability to separate in-plane and out-of-plane mechanical deformations via independent electrical interfaces to the four piezoresistive Si-NM elements. The schemes extend naturally to arrays of devices for spatiotemporal mapping of responses. Integration with wireless electronics yields a system that can interface with conventional consumer electronic platforms. This type of technology may provide utility in robotic interfaces, prosthetic control systems, medical diagnostics, and others.

RESULTS AND DISCUSSION

The fabrication exploits recent advances in the construction of 3D architectures, where doped Si-NMs integrate onto patterned films of polyimide (PI) that bond at selected locations to a prestrained elastomeric substrate. Transformation into 3D hierarchical shapes follows from compressive buckling induced by release of the prestrain (Figure 1a and Figure S1). The first step involves forming p-doped (boron) Si-NM piezoresistive

DOI: 10.1021/acsnano.9b02030
ACS Nano 2019, 13, 10972−10979

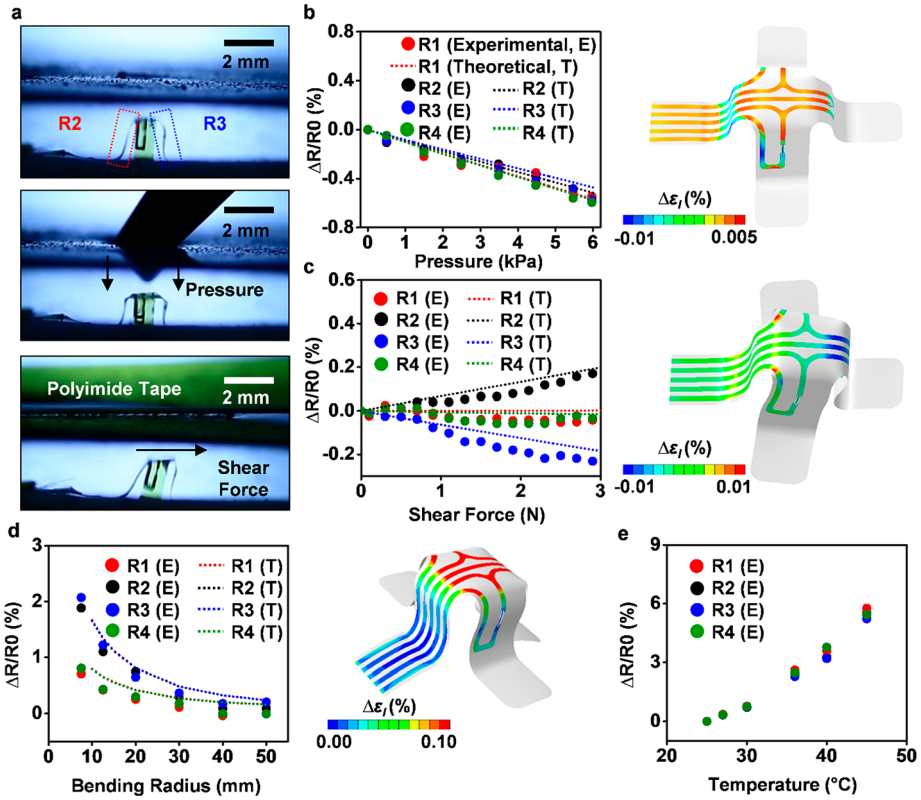

Figure 2. Characterization of the response of a sensor to normal pressure, shear force, bending, and temperature. (a) Optical images of an as-fabricated sensor (top) and in response to normal force (middle) and shear force (bottom). (b−e) Fractional change in resistance of four piezoresistive strain gauges as a function of normal pressure (b left), shear force (c left), bending force (d left), and temperature variation (e). The frames on the right show computed distributions of strain for such a system under a normal pressure of 6 kPa (b, right), a shear force of 10 N (c, right), and a bending radius of 10 mm curvature (d, right).

elements by impurity diffusion.[3,25,39] Here, a high doping concentration improves the quality of Ohmic contacts but reduces the gauge factor. Silicon with boron concentration of ~3 × 10^{19}/cm^3 (Figure S2a) represents a suitable balance for the present purposes, where the longitudinal piezoresistance factor is ~40% of that of silicon at a concentration of 1 × 10^6/cm^3.[40] Precise control of the diffusion temperature and time yields efficient doping in a reproducible manner (less than 10% variation of the mean value within a batch, Figure S2b).

The 2D precursor consists of two rectangular Si-NM piezoresistors positioned in the vertical direction (aligned head-to-tail and denoted as R2 and R3) and two more positioned in the horizontal direction (aligned head-to-tail and denoted as R1 and R4) (Figure 1b). Deposition of a bilayer of Ti/SiO_2 (5 nm/50 nm) on the backside of this platform through a shadow mask defines sites for strong bonding to a prestrained silicone substrate. The bonding here involves condensation reactions between the surface of the silicone, activated by exposure to ultraviolet-induced ozone, and the SiO_2 on the 2D precursor. Slow release of the prestrain transforms the 2D precursor into a 3D table-like configuration as shown in Figure 1c. Encapsulating the entire structure with a thin coating (~1 mm) of polydimethylsiloxane (PDMS) completes the process.

Here, the precise locations of the four Si-NM piezoresistive elements along the supporting legs strongly affect the measurement sensitivity. Positions near the bonding sites improve the shear force sensitivity at the cost of reduced pressure sensitivity (Figure S3). The current design, as detailed in the Methods, uses an optimal value for both responses to normal (~90% of maximum possible sensitivity) and shear (~50% of maximum possible sensitivity) forces. The overall lateral dimensions of the final device in this study are ~2 mm × ~2 mm, and the height is ~1 mm. These dimensions can be selected as necessary to address application requirements.

Responses of each of the piezoresistive elements in this 3D configuration yield separate electrical outputs that allow independent characterization of the stress tensor associated with applied force (Figure 2a). Figure 2b−d shows the output in terms of a fractional change in resistance ($\Delta R/R_0$) as a function of applied strain for three different loading conditions: normal force, shear force, and bending force. Under normal force (Figure 2b), identical compressive deformations at each of the four legs yield similar strain-induced changes in resistance in all four piezoresistive elements. The measured pressure and resistance values vary linearly with strain, with a slope of −0.1% kPa^{-1}, consistent with finite element analysis (FEA) results and a gauge factor of ~50 for the Si-NMs, similar to that reported for other silicon based electromechanical sensors.[3,25]

Uniaxial shear force applied along the direction from R2 to R3 in Figure 2c leads to tensile strain and a corresponding increase in resistance at R2, compressive strain and corresponding decrease in resistance at R3, with negligible strain, and change in resistance at R1 and R4. Here, the responses of the stretched and compressed legs are almost equal, ~0.07% N^{-1}, but differ by direction of the change in resistance, consistent with the direction of the shear force. Under the combined loading of pressure and shear force, the changes in resistance at R1−R4 correspond to linear superpositions of those when the load is

DOI: 10.1021/acsnano.9b02030
ACS Nano 2019, 13, 10972−10979

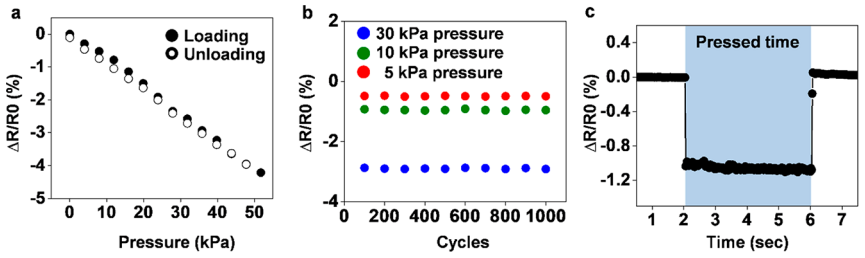

Figure 3. Evaluation of pressure and time responses and behavior under cyclic loading. (a) Response of a sensor to application and release of normal pressure loading. (b) Fractional change of resistance at different stages of fatigue testing, which involves 1000 cycles of loading to different normal pressures indicated in the legends. Three independent experiments yield similar results. (c) Measurements of the temporal response of a sensor.

applied separately and therefore can be used to determine the pressure and shear force simultaneously. Here, external stimuli can be modeled as

$$P = \frac{1}{2C_P}\left[\left(\frac{\Delta R}{R_0}\right)_2 + \left(\frac{\Delta R}{R_0}\right)_3\right] = \frac{1}{2C_P}\left[\left(\frac{\Delta R}{R_0}\right)_1 + \left(\frac{\Delta R}{R_0}\right)_4\right] \quad (1)$$

$$F_x = \frac{1}{2C_F}\left[\left(\frac{\Delta R}{R_0}\right)_2 - \left(\frac{\Delta R}{R_0}\right)_3\right] \quad \text{and}$$

$$F_y = \frac{1}{2C_F}\left[\left(\frac{\Delta R}{R_0}\right)_4 - \left(\frac{\Delta R}{R_0}\right)_1\right] \quad (2)$$

where $\left(\frac{\Delta R}{R_0}\right)_{1\sim4}$ are the fractional changes in resistance at R1−R4, P is the pressure, F is the shear force, and C_P and C_F are scaling factors for pressure and shear force, respectively. Fitting the measured data to the model yields $C_P \sim -0.1\%\ \text{kPa}^{-1}$ and $C_F \sim 0.07\%\ \text{N}^{-1}$, consistent with experimental data. FEA further suggests that linearity persists for pressure and shear forces up to ~200 kPa and ~10 N, within the fracture limit (1% of strain) at ~300 kPa and ~30 N, respectively (Figure S4). Under a convex bending condition (Figure 2d), all sensors experience tensile strain but with higher values for the two elements along the bending direction (R2 and R3) than those perpendicular (R1 and R4) to it.

Another parameter of interest is temperature, where the changes in resistance occur via both strains due to the thermal expansion of encapsulant and the temperature coefficient of resistance (TCR) of the Si-NMs. Figure 2e shows measured resistances of each of the four piezoresistive elements as a function of temperature. FEA based on the linear thermal expansion (3.2×10^{-4}/°C) of the encapsulant[41] yields strains of ~0.0035%/°C in the Si-NMs (Figure S5). The effective TCR determined for the complete system is $\sim 2.2 \times 10^{-3}$/°C, which is comparable to the sum of the effects associated with the intrinsic TCR of p-type silicon at a similar doping concentration[40] and those due to computed strains that arise from thermal expansion. Here, all four piezoresistive elements respond similarly, as expected.

This set of results demonstrates the mechanisms by which a single device responds differently to various external stimuli, with capabilities for measuring multiple types of sensory inputs. Decoupling of normal force (pressure) and shear force can be achieved by solving linear equations. Similarly decoupling bending, normal, and shear is not possible because the necessary five unknown parameters (one for pressure, two for shear, two for bending radii) cannot be obtained from four measured resistances. Furthermore, changes in temperature cannot be distinguished from normal pressure loading. The current device can, therefore, determine without ambiguity (1) pressure + shear forces and (2) temperature + shear forces. A revised design with an additional piezoresistive element, R5, at the center of the 3D structure may decouple simultaneous stimuli associated with shear forces, pressure, and temperature, as shown in the FEA results (see SI Section S1 for details).

Fast electrical and mechanical responses with minimal hysteresis are important for most practical applications. All constituent materials show approximately linear elastic behavior throughout the range of temperatures and mechanical forces of relevance for use in many human-interfaced systems (i.e., typical temperature and pressure ranges on human skin are 35−42 °C and 0−100 kPa,[3,42] respectively). Measurements of changes in resistance as a function of frequency during loading and unloading for many cycles under various pressures, all performed with a digital force gauge and multimeter (NI-USB 4065 Digital Multimeter), appear in Figure 3. The results show negligible hysteresis (<0.1%) upon loading and unloading, consistent with minimal effect of the viscoelasticity of the silicone encapsulant for these relatively high modulus materials (e.g., >100 GPa for Si-NM, ~2.5 GPa for PI[43]; Figure 3a). The sensor also exhibits good durability, with no variations in response over 1000 cycles under normal pressures of 5, 10, and 30 kPa (Figure 3b). The sensors respond quickly for loading/unloading under pressures from 5 to 30 kPa (0.2 ms sample rate; Figure S6). The immediate responses in the range of a few tens of milliseconds (Figure 3c and Figure S7) are in good agreement with previously reported sensors based on similar encapsulant and sensing materials.[3]

An interconnected 7 × 7 network of sensors with a unit cell size of ~2 × ~2 mm^2, distributed across an area of ~14 × ~14 mm^2 (Figure 4a and Figure S8), demonstrates the scalability of the fabrication process, particularly relevant for applications that require capture of spatial distributions of stimuli. Here, the compressive 3D buckling process transforms all sensors into 3D configurations simultaneously, with resulting distributions of material strains (~0.4% in gold, 0.15% in Si) that are similar to those of isolated sensors described previously (Figure S9). Figure 4b,c shows the operation of the array with a glass tube (inner diameter, ~15 mm; outer diameter, ~17 mm; weight, 35 g) positioned on top of the sensors. The resulting pressure induces compressive deformation at the outer sensors and corresponding negative changes of resistance, while tensile strain by the local shear force toward the tube location results in positive changes of resistance at the inner sensors (Figure 4c).

DOI: 10.1021/acsnano.9b02030
ACS Nano 2019, 13, 10972−10979

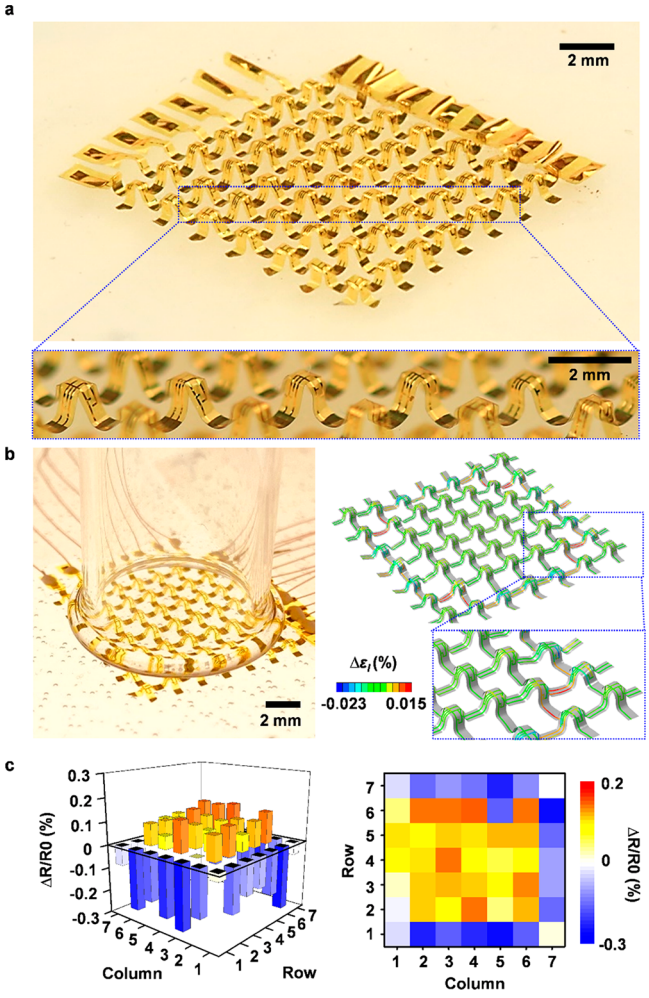

Figure 4. Large-area integration. (a) Optical image of a 7 × 7 sensor array and magnified views of unit cells (inset) designed to measure the spatial distribution of external loads. (b) Left, image of the device with a glass tube placed on top. Right, corresponding finite element analysis results that define distributions of strain and 3D geometries. (c) The resulting changes in resistance measured across the array in three-dimensional (left) and two-dimensional (right) renderings.

FEA modeling further confirms the similar spatial distribution with negative (~0.23–0.35%) and positive (~0.01–0.08%) resistance changes at outer and inner sensors, respectively (Figure S10). The color contrast clearly indicates the local pressure and shear force distributions, consistent with the shape of the glass tube.

Electrically integrating this type of sensor with a wireless electronics module (Bluetooth) yields a tether-free measurement system with large operating range suitable for various applications (Figure 5a,b). The fabrication approach integrates the sensors with flexible printed circuit boards (flex-PCBs) as supports for active and passive electronic components, such as batteries, Bluetooth chips, power regulators, amplifiers, capacitors, and resistors. Here, the platform utilizes the nRF52832 Bluetooth Low Energy protocol, a Li-ion 12 mAh battery (10 h operation lifetime), and a Low Dropout (LDO) power converter which regulates the 4.2 V output of the battery to 3.3 V (Figure S11). The platform uses four analog to digital converters (ADCs), each of which operates with a 0.6 V reference voltage and 14-bit resolution, to measure changes in

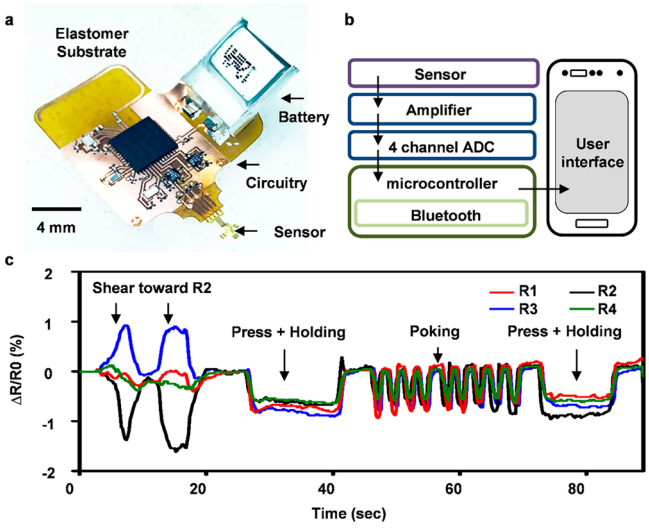

Figure 5. Wireless data acquisition. (a) Optical micrograph of a 3D sensor integrated with a wireless electronics module, including flexible printed circuit board, surface-mounted electronic components, and silicone substrate/encapsulant. (b) Operational block diagram of the overall wireless platform design. A Bluetooth controller transmits sensor measurements for real-time data readout and logging on a smartphone or tablet computer. (c) Wirelessly recorded sensing data show responses to shear force and normal pressure.

resistance of the four piezoelectric elements. Subtle changes in resistance (~1%) created by external stimuli convert into changes in voltage via a voltage divider with reference resistor. The device also has four gain amplifiers set to a gain of 1. These settings can be modified for applications that require high sensitivity to low pressure. A custom circuit simulator and data analysis software package allow for fine-tuning of the circuit before integration. Figure 5c presents wirelessly recorded and recalculated fractional changes of resistance in response to shear and normal applied force.

CONCLUSION

The results described here illustrate methods for integrating silicon piezoresistive elements into 3D configurations for multimodal sensors with the ability to respond to various stimuli associated with interactions with a physical environment. Specifically, the outputs yield simultaneous, independent information on pressure, shear and bending deformations, and temperature. The schemes scale naturally to arrays of devices for mapping purposes. In all cases, the operation is compatible with standard Bluetooth electronics, thereby enabling collection, transmission, and analysis of data in a fully wireless manner, compatible with envisioned applications in health monitors, biomedical devices, and human-robotic devices. This system and a set of demonstration studies suggest opportunities for the use of 3D dynamic platforms in sensors/actuators as the basis for advanced biomedical and/or health monitoring technologies.

METHODS

Device Fabrication. Boron doping (1000 °C, 10 min) defined areas across the device silicon layer of a silicon on an insulator wafer (SOI, top silicon ~200 nm, SOITEC INC) as active regions for piezoresistive sensing. Removal of the buried silicon oxide layer with hydrofluoric acid (HF) released the top silicon layer from the mother wafer, thereby enabling transfer printing of the resulting Si-NMs onto a

DOI: 10.1021/acsnano.9b02030
ACS Nano 2019, 13, 10972–10979

receiver substrate composed of a layer of PI (~4 μm, HD microsystems INC) on a layer of PMMA (~100 nm, MicroChem INC) on a glass slide. Photolithography followed by reactive ion etching (RIE, SF_6, 30 mTorr, 50 W, 20 sccm, 200 s) and electron beam evaporation (Cr/Au, 5/200 nm) yielded defined silicon elements and metal interconnects, respectively. Coating a thin layer of PI (~2.5 μm) as a passivation layer and forming a mesh structure by RIE (O_2, 100 mTorr, 100 W, 20 sccm, 15 min) completed the formation of a 2D precursor. Dissolving the PMMA layer with acetone released the structure from the wafer. Retrieving this precursor onto a PDMS stamp and evaporating layers of Ti/SiO_2 (5/100 nm) selectively onto bonding sites on the exposed backside surface prepared the system for a covalent bonding onto a prestrained silicone elastomer pretreated by exposure to UVO (5 min). Releasing the prestrain led to geometrical transformation of the 2D precursor into a 3D configuration. Application of a coating of PDMS (~1 mm) completed the fabrication.

Measurement Setting. The measurement setup consisted of a customized vertical and horizontal stage used with a force gauge (Mark-10) and digital multimeters (NI-USB 4065 Digital Multimeter) for the electrical resistance measurement. For shear force measurement, the sensor was secured at its base and the force gauge was used to pull a film of PI (width of ~1 cm) adhered to the top surface of the sensor.

Finite Element Analysis. FEA was conducted to study the buckled 3D shapes and strains in silicon, gold, and PI, using the commercial software ABAQUS (version 6.14, Standard). FEA involved two steps: (1) transformation from the 2D precursor to the 3D architecture without the encapsulation and (2) addition of the encapsulation, thereby coupling deformations of the encapsulation to those of the 3D structure. The 3D structure, elastomeric substrate, and encapsulation were modeled by the four-node finite-strain shell element and eight-node and four-node solid elements, respectively. Mesh refinement (e.g., at least 20 elements along the longitudinal direction of the piezoresistors; extremely fine mesh in the encapsulation surrounding the 3D structure; >1 million elements) ensured accuracy. PI, silicon, and gold were linear elastic with the Young's modulus E and Poisson's ratio ν: E_{PI} = 2.5 GPa, ν_{PI} = 0.34, E_{Si} = 130 GPa, ν_{Si} = 0.27, E_{Au} = 78 GPa, and ν_{Au} = 0.44. The elastomeric substrate and encapsulation were Ecoflex and PDMS, respectively, with Young's modulus and Poisson's ratio $E_{Ecoflex}$ = 60 kPa, $\nu_{Ecoflex}$ = 0.49, E_{PDMS} = 2 MPa, and ν_{PDMS} = 0.49 in the Mooney-Rivlin Hyperelastic model. The corresponding parameters in the Mooney-Rivlin model were $C_{10Ecoflex}$ = 8.1 kPa, $C_{01Ecoflex}$ = 2.0 kPa, $D_{1Ecoflex} = 2.0 \times 10^{-6}$ Pa^{-1}, C_{10PDMS} = 270 kPa, C_{01PDMS} = 67 kPa, and $D_{1PDMS} = 6.0 \times 10^{-8}$ Pa^{-1}. The relative resistance change $\frac{\Delta R}{R_0}$ is related to the strain via $\frac{\Delta R}{R_0} = G\varepsilon_l$, where ε_l is the strain in the longitudinal direction of the piezoresistors (Si-NMs) and G is the gauge factor. The loading conditions for the simulation results in the main text are (1) a uniform pressure in a circular area with 8 mm radius on the top surface of the encapsulation for Figure 2b (Figure S4a), (2) uniform shear forces on the entire top surface of the encapsulation for Figure 2c (Figure S4b), (3) rotation boundary conditions at two sides of the encapsulation for Figure 2d (Figure S4c), and (4) a uniform pressure in a ring area with 7.5 mm inner radius and 8.5 mm outer radius (Figure S10).

Simultaneous Determination of Pressure and Shear Forces. Under pressure P, the relative resistance changes $\frac{\Delta R}{R_0}$ in the piezoresistors R1−4 are

$$\left(\frac{\Delta R}{R_0}\right)_{1\sim4} = C_P P \tag{3}$$

where $C_P \approx -0.1\%$/kPa (slope in Figure 2b) and R_0 is the resistance without pressure. Under shear force F_x along the x-direction, the resistance changes are

$$\left(\frac{\Delta R}{R_0}\right)_2 = -\left(\frac{\Delta R}{R_0}\right)_3 = C_F F_x, \quad \left(\frac{\Delta R}{R_0}\right)_1 = -\left(\frac{\Delta R}{R_0}\right)_4 = 0 \tag{4}$$

where $C_F \approx 0.07\%$/N (slope in Figure 2c). Similarly, under shear force F_y along the y-direction,

$$\left(\frac{\Delta R}{R_0}\right)_4 = -\left(\frac{\Delta R}{R_0}\right)_1 = C_F F_y, \quad \left(\frac{\Delta R}{R_0}\right)_2 = \left(\frac{\Delta R}{R_0}\right)_3 = 0 \tag{5}$$

When the pressure P and shear forces F_x, F_y are applied simultaneously, the resistance changes are the linear superposition of eqs 3−5 for small deformation. Therefore, P, F_x, and F_y can be determined from $\left(\frac{\Delta R}{R_0}\right)_{1\sim4}$ as in eq 1 and eq 2.

Optimization of the Piezoresistor Locations. The piezoresistive elements are located near the middle of each leg based on the balance of sensitivity to pressure (C_P) and shear force (C_F). A parametric study was performed by FEA, with the piezoresistive element located by its normalized distance to the bonding site (D/L in Figure S3a). $|C_P|$ takes its maximum value when D/L = 0.2 (Figure S3b), while $|C_F|$ increases when D/L decreases (i.e., closer to the bonding site, Figure S3c). The design reported in the main text takes $D/L \approx 0.22$ such that $|C_P|$ and $|C_F|$ are ~90% and ~50% of the maximum, respectively.

Array Wiring Scheme. Each unit cell has two piezoresistive elements (Figure S8). An additional interdielectric layer (PI 2545; HD Microsystem) separates the first and second metal layers for data and bias lines, respectively. The read-out circuit for a piezoresistive element in the array consists of an operational amplifier that is electrically integrated at each column terminal to reduce crosstalk current, as detailed elsewhere.[44−46] Each unit cell is read sequentially with a digital multimeter (NI-USB 4065 Digital Multimeter).

ASSOCIATED CONTENT

Supporting Information

The Supporting Information is available free of charge on the ACS Publications website at DOI: 10.1021/acsnano.9b02030.

Supplementary note describing finite element analysis and analytical modeling for simultaneous determination of pressure, shear force, and temperature and figures including details of finite elemental analysis modeling, fabrication process, frequency responses to various pressure inputs, fabrication of a sensor array, layout information for the wireless electronics, and design with five sensing elements for simultaneous measurement of temperature pressure and shear forces (PDF)

Movie showing single buckling (AVI)

Movie showing array buckling (AVI)

AUTHOR INFORMATION

Corresponding Author

*(J.A.R.) E-mail: jrogers@northwestern.edu.

ORCID

Bong Hoon Kim: 0000-0002-4610-0176

Kaitlyn E. Crawford: 0000-0001-7396-6349

Yihui Zhang: 0000-0003-0885-2067

John A. Rogers: 0000-0002-2980-3961

Author Contributions

&S. M. Won, H. Wang, B. H. Kim, and K. Lee contributed equally to this work.

Notes

The authors declare no competing financial interest.

ACKNOWLEDGMENTS

Y.Z. acknowledges the support from the National Natural Science Foundation of China (No. 11722217) and the Tsinghua National Laboratory for Information Science and Technology. Y.H. acknowledges the support from the NSF (No.

CMMI1400169, CMMI1534120, and CMMI1635443). S.H. was supported by the National Research Foundation of Korea (NRF) grant funded by the Korean government (No. 2019R1C1C1007629) and the Ajou University research fund. Y.S.O. was supported by the Basic Science Research Program (N01180787) of the National Research Foundation of Korea (NRF) funded by the Ministry of Education. B.H.K. was supported by the Competency Development Program for Industry Specialists (No. P0002397, HRD program for Industrial Convergence of Wearable Smart Devices) of the Korean Ministry of Trade, Industry and Energy (MOTIE), operated by Korea Institute for Advancement of Technology (KIAT) and Nano·Material Technology Development Program (2009-0082580) through the National Research Foundation of Korea (NRF) funded by the Ministry of Science, ICT and Future Planning.

REFERENCES

(1) Khan, Y.; Ostfeld, A. E.; Lochner, C. M.; Pierre, A.; Arias, A. C. Monitoring of Vital Signs with Flexible and Wearable Medical Devices. *Adv. Mater.* **2016**, *28*, 4373−4395.

(2) Gao, Y.; Ota, H.; Schaler, E. W.; Chen, K.; Zhao, A.; Gao, W.; Fahad, H. M.; Leng, Y.; Zheng, A.; Xiong, F.; Zhang, C.; Tai, L.-C.; Zhao, P.; Fearing, R. S.; Javey, A. Wearable Microfluidic Diaphragm Pressure Sensor for Health and Tactile Touch Monitoring. *Adv. Mater.* **2017**, *29*, 1701985.

(3) Han, S.; Kim, J.; Won, S. M.; Ma, Y.; Kang, D.; Xie, Z.; Lee, K.-T.; Chung, H. U.; Banks, A.; Min, S.; Heo, S. Y.; Davies, C. R.; Lee, J. W.; Lee, C.-H.; Kim, B. H.; Li, K.; Zhou, Y.; Wei, C.; Feng, X.; Huang, Y.; et al. Battery-Free, Wireless Sensors for Full-Body Pressure and Temperature Mapping. *Sci. Transl. Med.* **2018**, *10*, No. eaan4950.

(4) Liu, Y.; Wang, H.; Zhao, W.; Zhang, M.; Qin, H.; Xie, Y. Flexible, Stretchable Sensors for Wearable Health Monitoring: Sensing Mechanisms, Materials, Fabrication Strategies and Features. *Sensors* **2018**, *18*, 645.

(5) Wu, Y.; Liu, Y.; Zhou, Y.; Man, Q.; Hu, C.; Asghar, W.; Li, F.; Yu, Z.; Shang, J.; Liu, G.; Liao, M.; Li, R.-W. A Skin-Inspired Tactile Sensor for Smart Prosthetics. *Sci. Robot.* **2018**, *3*, No. eaat0429.

(6) Toyama, S.; Tanaka, Y.; Shirogane, S.; Nakamura, T.; Umino, T.; Uehara, R.; Okamoto, T.; Igarashi, H. Development of Wearable Sheet-Type Shear Force Sensor and Measurement System that is Insusceptible to Temperature and Pressure. *Sensors* **2017**, *17*, 1752.

(7) Boutry, C. M.; Negre, M.; Jorda, M.; Vardoulis, O.; Chortos, A.; Khatib, O.; Bao, Z. A Hierarchically Patterned, Bioinspired E-skin Able to Detect the Direction of Applied Pressure for Robotics. *Sci. Robot.* **2018**, *3*, No. eaau6914.

(8) Hua, Q.; Sun, J.; Liu, H.; Bao, R.; Yu, R.; Zhai, J.; Pan, C.; Wang, Z. L. Skin-Inspired Highly Stretchable and Conformable Matrix Networks for Multifunctional Sensing. *Nat. Commun.* **2018**, *9*, 244.

(9) Larson, C.; Peele, B.; Li, S.; Robinson, S.; Totaro, M.; Beccai, L.; Mazzolai, B.; Shepherd, R. Highly Stretchable Electroluminescent Skin for Optical Signaling and Tactile Sensing. *Science* **2016**, *351*, 1071−1074.

(10) You, I.; Choi, S.-E.; Hwang, H.; Han, S. W.; Kim, J. W.; Jeong, U. E-Skin Tactile Sensor Matrix Pixelated by Position-Registered Conductive Microparticles Creating Pressure-Sensitive Selectors. *Adv. Funct. Mater.* **2018**, *28*, 1801858.

(11) Lai, Y.-C.; Deng, J.; Liu, R.; Hsiao, Y.-C.; Zhang, S. L.; Peng, W.; Wu, H.-M.; Wang, X.; Wang, Z. L. Actively Perceiving and Responsive Soft Robots Enabled by Self-Powered, Highly Extensible, and Highly Sensitive Triboelectric Proximity- and Pressure-Sensing Skins. *Adv. Mater.* **2018**, *30*, 1801114.

(12) Cao, R.; Pu, X.; Du, X.; Yang, W.; Wang, J.; Guo, H.; Zhao, S.; Yuan, Z.; Zhang, C.; Li, C.; Wang, Z. L. Screen-Printed Washable Electronic Textiles as Self-Powered Touch/Gesture Tribo-Sensors for Intelligent Human-Machine Interaction. *ACS Nano* **2018**, *12*, 5190−5196.

(13) Li, J.; Orrego, S.; Pan, J.; He, P.; Kang, S. H. Ultrasensitive, Flexible, and Low-Cost Nanoporous Piezoresistive Composites for Tactile Pressure Sensing. *Nanoscale* **2019**, *11*, 2779−2786.

(14) Wu, Y.; Karakurt, I.; Beker, L.; Kubota, Y.; Xu, R.; Ho, K. Y.; Zhao, S.; Zhong, J.; Zhang, M.; Wang, X.; Lin, L. Piezoresistive Stretchable Strain Sensors with Human Machine Interface Demonstrations. *Sens. Actuators, A* **2018**, *279*, 46−52.

(15) Choi, D.; Jang, S.; Kim, J. S.; Kim, H.-J.; Kim, D. H.; Kwon, J.-Y. A Highly Sensitive Tactile Sensor Using a Pyramid-Plug Structure for Detecting Pressure, Shear Force, and Torsion. *Adv. Mater. Technol.* **2019**, *4*, 1800284.

(16) Pang, C.; Lee, G.-Y.; Kim, T.-I.; Kim, S. M.; Kim, H. N.; Ahn, S.-H.; Suh, K.-Y. A Flexible and Highly Sensitive Strain-Gauge Sensor Using Reversible Interlocking of Nanofibres. *Nat. Mater.* **2012**, *11*, 795−801.

(17) Gong, S.; Schwalb, W.; Wang, Y.; Chen, Y.; Tang, Y.; Si, J.; Shirinzadeh, B.; Cheng, W. A Wearable and Highly Sensitive Pressure Sensor with Ultrathin Gold Nanowires. *Nat. Commun.* **2014**, *5*, 3132−3139.

(18) Kim, J.; Lee, M.; Shim, H. J.; Ghaffari, R.; Cho, H. R.; Son, D.; Jung, Y. H.; Soh, M.; Choi, C.; Jung, S.; Chu, K.; Jeon, D.; Lee, S.-T.; Kim, J. H.; Choi, S. H.; Hyeon, T.; Kim, D.-H. Stretchable Silicon Nanoribbon Electronics for Skin Prosthesis. *Nat. Commun.* **2014**, *5*, 5747.

(19) Park, K.-I.; Son, J. H.; Hwang, G.-T.; Jeong, C. K.; Ryu, J.; Koo, M.; Choi, I.; Lee, S. H.; Byun, M.; Wang, Z. L.; Lee, K. J. Highly-Efficient, Flexible Piezoelectric PZT Thin Film Nanogenerator on Plastic Substrates. *Adv. Mater.* **2014**, *26*, 2514−2520.

(20) Wang, N.; Dou, W.; Hao, S.; Cheng, Y.; Zhou, D.; Huang, X.; Jiang, C.; Cao, X. Tactile Sensor from Self-Chargeable Piezoelectric Supercapacitor. *Nano Energy* **2019**, *56*, 868−874.

(21) Lee, S.; Reuveny, A.; Reeder, J.; Lee, S.; Jin, H.; Liu, Q.; Yokota, T.; Sekitani, T.; Isoyama, T.; Abe, Y.; Suo, Z.; Someya, T. A Transparent Bending-Insensitive Pressure Sensor. *Nat. Nanotechnol.* **2016**, *11*, 472−478.

(22) Pu, X.; Liu, M.; Chen, X.; Sun, J.; Du, C.; Zhang, Y.; Zhai, J.; Hu, W.; Wang, Z. L. Ultrastretchable, Tranparent Triboelectric Nanogenerator as Electronic Skin for Biomechanical Energy Harvesting and Tactile Sensing. *Sci. Adv.* **2017**, *3*, No. e1700015.

(23) Tao, J.; Bao, R.; Wang, X.; Peng, Y.; Li, J.; Fu, S.; Pan, C.; Wang, Z. L. Self-Powered Tactile Sensor Array Systems Based on the Triboelectric Effect. *Adv. Funct. Mater.* **2018**, 1806379.

(24) Bu, T.; Xiao, T.; Yang, Z.; Liu, G.; Fu, X.; Nie, J.; Guo, T.; Pang, Y.; Zhao, J.; Xi, F.; Zhang, C.; Wang, Z. L. Stretchable Triboelectric-Photonic Smart Skin for Tactile and Gesture Sensing. *Adv. Mater.* **2018**, *30*, 1800066.

(25) Kang, S.-K.; Murphy, R. K. J.; Hwang, S.-W.; Lee, S. M.; Harburg, D. V.; Krueger, N. A.; Shin, J.; Gamble, P.; Cheng, H.; Yu, S.; Liu, Z.; McCall, J. G.; Stephen, M.; Ying, H.; Kim, J.; Park, G.; Webb, R. C.; Lee, C. H.; Chung, S.; Wie, D. S.; et al. Bioresorbable Silicon Electronic Sensors for the Brain. *Nature* **2016**, *530*, 71−76.

(26) Kwon, D.; Lee, T.-I.; Shim, J.; Ryu, S.; Kim, M. S.; Kim, S.; Kim, T.-S.; Park, I. Highly Sensitive, Flexible, and Wearable Pressure Sensor Based on a Giant Piezocapacitive Effect of Three-Dimensional Microporous Elastomeric Dielectric Layer. *ACS Appl. Mater. Interfaces* **2016**, *8*, 16922−16931.

(27) Ponce Wong, R. D.; Posner, J. D.; Santos, V. J. Flexible Microfluidic Normal Force Sensor Skin for Tactile Feedback. *Sens. Actuators, A* **2012**, *179*, 62−69.

(28) Li, B.; Fontecchio, A. K.; Visell, Y. Mutual Capacitance of Liquid Conductors in Deformable Tactile Sensing Arrays. *Appl. Phys. Lett.* **2016**, *108*, 013502.

(29) Jeong, Y. R.; Kim, J.; Xie, Z.; Xue, Y.; Won, S. M.; Lee, G.; Jin, S. W.; Hong, S. Y.; Feng, X.; Huang, Y.; Rogers, J. A.; Ha, J. S. A Skin-Attachable, Stretchable Integrated System Based on Liquid GaInSn for Wireless Human Motion Monitoring with Multi-Site Sensing Capabilities. *NPG Asia Mater.* **2017**, *9*, No. e443.

(30) Segev-Bar, M.; Haick, H. Flexible Sensors Based on Nanoparticles. *ACS Nano* **2013**, *7*, 8366−8378.

DOI: 10.1021/acsnano.9b02030
ACS Nano 2019, 13, 10972−10979

(31) Takei, K.; Yu, Z.; Zheng, M.; Ota, H.; Takahashi, T.; Javey, A. Highly Sensitive Electronic Whiskers Based on Patterned Carbon Nanotube and Silver Nanoparticle Composite Films. *Proc. Natl. Acad. Sci. U. S. A.* **2014**, *111*, 1703−1707.
(32) Kim, H.; Kim, G.; Kim, T.; Lee, S.; Kang, D.; Hwang, M.-S.; Chae, Y.; Kang, S.; Lee, H.; Park, H.-G.; Shim, W. Transparent, Flexible, Conformal Capacitive Pressure Sensors with Nanoparticles. *Small* **2018**, *14*, 1703432.
(33) An, B. W.; Heo, S.; Ji, S.; Bien, F.; Park, J.-U. Transparent and Flexible Fingerprint Sensor Array with Multiplexed Detection of Tactile Pressure and Skin Temperature. *Nat. Commun.* **2018**, *9*, 2458.
(34) Kim, B. H.; Lee, J.; Won, S. M.; Xie, Z.; Chang, J.-K.; Yu, Y.; Cho, Y. K.; Jang, H.; Jeong, J. Y.; Lee, Y.; Ryu, A.; Kim, D. H.; Lee, K. H.; Lee, J. Y.; Liu, F.; Wang, X.; Huo, Q.; Min, S.; Wu, D.; Ji, B.; et al. Three-Dimensional Silicon Electronic Systems Fabricated by Compressive Buckling Process. *ACS Nano* **2018**, *12*, 4164−4171.
(35) Kim, B. H.; Liu, F.; Yu, Y.; Jang, H.; Xie, Z.; Li, K.; Lee, J.; Jeong, J. Y.; Ryu, A.; Lee, Y.; Kim, D. H.; Wang, X.; Lee, K.; Lee, J. Y.; Won, S. M.; Oh, N.; Kim, J.; Kim, J. Y.; Jeong, S.-J.; Jang, K.-I.; et al. Mechanically Guided Post-Assembly of 3D Electronic Systems. *Adv. Funct. Mater.* **2018**, *28*, 1803149.
(36) Nan, K.; Kang, S. D.; Li, K.; Yu, K. J.; Zhu, F.; Wang, J.; Dunn, A. C.; Zhou, C.; Xie, Z.; Agne, M. T.; Wang, H.; Luan, H.; Zhang, Y.; Huang, Y.; Snyder, G. J.; Rogers, J. A. Compliant and Stretchable Thermoelectric Coils for Energy Harvesting in Miniature Flexible Devices. *Sci. Adv.* **2018**, *4*, No. eaau5849.
(37) Nan, K.; Wang, H.; Ning, X.; Miller, K. A.; Wei, C.; Liu, Y.; Li, H.; Xue, Y.; Xie, Z.; Luan, H.; Zhang, Y.; Huang, Y.; Rogers, J. A.; Braun, P. V. Soft Three-Dimensional Microscale Vibratory Platforms for Characterization of Nano-Thin Polymer Films. *ACS Nano* **2019**, *13*, 449−457.
(38) Zhang, Y.; Zhang, F.; Yan, Z.; Ma, Q.; Li, X.; Huang, Y.; Rogers, J. A. Printing, Folding and Assembly Methods for Forming 3D Mesostructures in Advanced Materials. *Nat. Rev. Mater.* **2017**, *2*, 17019.
(39) Won, S. M.; Kim, H.; Lu, N.; Kim, D.; Del Solar, C.; Duenas, T.; Ameen, A.; Rogers, J. A. Piezoresistive Strain Sensors and Multiplexed Arrays Using Assemblies of Single-Crystalline Silicon Nanoribbons on Plastic Substrates. *IEEE Trans. Electron Devices* **2011**, *58*, 4074−4078.
(40) Doll, J. C.; Pruitt, B. L. *Piezoresistor Design and Application*; Springer: New York, NY, U.S.A., 2013; pp 21−148.
(41) Xu, S.; Yan, Z.; Jang, K.-I.; Huang, W.; Fu, H.; Kim, J.; Wei, Z.; Flavin, M.; McCracken, J.; Wang, R.; Badea, A.; Liu, Y.; Xiao, D.; Zhou, G.; Lee, J.; Chung, H. U.; Cheng, H.; Ren, W.; Banks, A.; Li, X.; et al. Assembly of Micro/Nanomaterials into Complex, Three-Dimensional Architectures by Compressive Buckling. *Science* **2015**, *347*, 154−159.
(42) Zang, Y.; Zhang, F.; Di, C.-A.; Zhu, D. Advances of Flexible Pressure Sensors Toward Artificial Intelligence and Health Care Applications. *Mater. Horiz.* **2015**, *2*, 140−156.
(43) Schubert, B. E.; Floreano, D. Variable Stiffness Material Based on Rigid Low-Melting-Point-Alloy Microstructures Embedded in Soft Poly(dimethylsiloxane) (PDMS). *RSC Adv.* **2013**, *3*, 24671−24679.
(44) Castellanos-Ramos, J.; Navas-Gonzalez, R.; Macicior, H.; Sikora, T.; Ochoteco, E.; Vidal-Verdu, F. Tactile Sensors Based on Conductive Polymers. *Microsyst. Technol.* **2010**, *16*, 765−776.
(45) Kim, J.-S.; Kwon, D.-Y.; Choi, B.-D. High-Accuracy, Compact Scanning Method and Circuit for Resistive Sensor Arrays. *Sensors* **2016**, *16*, 155.
(46) Sun, X.; Wang, C.; Chi, C.; Xue, N.; Liu, C. A Highly-Sensitive Flexible Tactile Sensor Array Utilizing Piezoresistive Carbon Nanotube-Polydimethylsiloxane Composite. *J. Micromech. Microeng.* **2018**, *28*, 105011.

DOI: 10.1021/acsnano.9b02030
ACS Nano 2019, 13, 10972−10979